Role of Counterion Condensation in the Self-Assembly of SDS Surfactants at the Water−Graphite Interface

Naga Rajesh Tummala and Alberto Striolo*

The University of Oklahoma School of Chemical Biological and Materials Engineering, Norman, Oklahoma 73019

Received: September 24, 2007; In Final Form: November 17, 2007

The aggregate structure of sodium dodecyl sulfate (SDS) adsorbed at the graphite−water interface has been studied with the aid of molecular dynamics (MD) simulations. As expected, our results show that adsorbed SDS yields hemi-cylindrical micelles. The hemi-cylindrical aggregates in our simulations closely resemble all structural and morphological details provided by previous solution atomic force microscopy (AFM) experiments. More interestingly, our data indicate that SDS head groups do not provide a complete shield to the hydrophobic tails. Instead, we found regions in which the hydrophobic tails are exposed to the aqueous solution. By conducting a parametric study for SDS-like nonionic surfactants we show that electrostatic interactions between SDS head groups and counterions are responsible for the unexpected result. Our interpretation is corroborated by density profiles, analysis of the coordination states, and mean square displacement data for both the adsorbed SDS surfactants and the counterions in solution. Counterion condensation appears to be a physical phenomenon that could be exploited to direct the assembly of advanced nanostructured materials.

1. Introduction

Amphiphilic molecules are used in a variety of applications that employ their ability to self-assemble, including fabrication of porous materials,[1] structured materials,[2] and also tuning the effective interactions between latex spheres in aqueous solution.[3] Surfactants are amphiphilic molecules with relatively long (8−24 carbon atoms) hydrophobic tails and short hydrophilic heads. Studies of surfactant adsorption on solid surfaces date back to the 1960s and the classic papers of Furstenau.[4−8] Because of the commercial importance of applications such as mineral flotation processes and detergency, many pioneering studies focused on surfactant adsorption on small particulate solids.[9−18] Development of atomic force microscopy (AFM) promoted a significant breakthrough in the area of surfactant adsorption. The results from AFM experiments during the 1990s revealed the hemi-cylindrical aggregate structure of ionic surfactants on hydrophobic substrates.[19−22] It is now clear that the morphology of surfactants self-assembled structures varies as the critical packing shape and available surface area for the amphiphilic molecule change.[23] A number of amphiphilic molecules are known which self-assemble yielding bilayers, hemi-cylinders, and hemi-spheres.

The structural properties of surfactant systems have been investigated via theoretical techniques.[24,25] Leermakers and co-workers[26−29] discussed in a series of articles the results obtained from self-consistent field theory (SCF) for surfactants confined between surfaces. The calculations suggest that for ionic surfactants on amphiphilic surfaces at close enough separation distances (e.g., the removal point) one of the two adsorbed layers desorbs due to the presence of the other. In addition, at distances smaller than the removal point, the amount of surfactant adsorbed on one surface is larger than not only that adsorbed on the other surface but also than that on a free-standing surface. Thus, frontal confinement affects how much surfactant is adsorbed at wall−wall separations comparable to the surfactant length. Simulations have been performed at a coarse-grained (CG) level to describe, for example, bulk surfactant solutions[30] or the adsorption of anionic surfactants,[31] and that of diblock copolymers[32,33] on solid surfaces, either homogeneous or heterogeneous.[34−40] CG simulations provide general trends, such as the dependency of the adsorbed amount and adsorbate structure on the adsorption energy and the head/tail ratio.[41−52] Wijmans and Linse showed that self-assembly at the surface occurs at bulk concentrations lower than the critical micelle concentration (CMC)[31] because the surfactant concentration is higher near the surface than it is in the bulk solution. Also, the adsorption isotherm on a surface presents a plateau when the bulk concentration is larger than CMC.[53] All-atom simulations are required within molecular dynamics (MD) algorithms[54,55] to better understand the molecular-level mechanism of interfacial phenomena related to surfactant aggregation. It should however be clear that the current computing infrastructures allow researchers to conduct all-atom MD studies for only up to a few tens of nanoseconds. Despite this limitation, all-atom MD can be used, for example, to study surfactants at air−water[56] and water−CCl_4 interfaces,[57] the structure of reverse micelles,[58] the adsorption of surfactants on scheelite,[59] or the self-assembly of water/surfactant/CO_2 systems.[60−62] Shah et al. studied aqueous solutions of *n*-dodecyltrimethylammonium bromide in contact with hydrophilic silica surfaces.[63] The authors were able to show that the compact spherical or elliptical micellar structure observed for the surfactants in bulk solution evolves to flat elliptical structures at contact with silica surfaces, in agreement with experiments. Bandyopadhyay et al. showed that cetyltrimethylammonium bromide (CTAB) surfactants on graphite form stable hemi-cylindrical aggregates, in agreement with experimental observations.[64] Dominguez recently reported MD

* To whom correspondence should be addressed. Phone: 405 325 5716. Fax: 405 325 5813. E-mail: astriolo@ou.edu.

10.1021/jp077678m CCC: $40.75 © 2008 American Chemical Society
Published on Web 01/30/2008

simulation results for sodium dodecyl sulfate (SDS) surfactants at graphite−water interfaces.[65] The results show the formation of hemi-cylinders at surface coverage of 0.45 nm^2 per head group and full cylinders with water near the graphite surface at surface coverage of 0.20 nm^2. Bruce et al.[66] provided data for the distribution of counterions in SDS micelles in solution.

We are here interested in the morphology of SDS self-assembled aggregates at the graphite−water interface. We monitor the relative arrangement of surfactant heads and surfactant tails (which is difficult, at best, to obtain experimentally), the role of counterion condensation on the surface aggregate morphology, and the effect of frontal confinement in the structure and dynamics of the self-assembled structures. Our results compare semiquantitatively to AFM experimental data provided by Wanless and Ducker,[22] which show that hemicylindrical structures form at bulk concentration well below the CMC and that the periodicity of the surface aggregates changes with the concentration of salts in solution and decreases as the SDS concentration increases. In section 2 we provide simulation details and algorithms, in section 3 we discuss our main results, and in section 4 we summarize our conclusions.

2. Simulation Methodology

Our goal is to study the morphology of SDS aggregates at the graphite−water interface. The entire process of surfactant adsorption from solution cannot be simulated by standard all-atom MD techniques within the limitations of the current computational resources. In fact, the typical time scale for surfactant adsorption/desorption from a micelle is ∼1 μs.[24] Thus, it is customary to arrange a given number of surfactant molecules on a surface and then conduct MD simulations to assess their equilibrium properties.[64,65] Because the results depend on the surfactants surface density, it is necessary to employ experimentally relevant data to initiate the MD calculations. Optical measurements for SDS on graphon indicate that the surface area per head group is ∼0.40 nm^2 at a bulk concentration of 7 mM SDS.[67] This is the surface area per head group considered in this work. To increase statistical accuracy, two opposing graphite surfaces were considered to gather most of the results discussed below. Sufficient SDS molecules were placed on each graphite surface, and water, with sodium counterions, was placed in the region between them. The overall density between the graphite surfaces was ∼0.94 g/cc, and the water density at the center of the simulation box was ∼1.0 g/cc.

Water was simulated using the simple point charge/extended (SPC/E) model.[68] Carbon atoms in highly ordered pyrolitic graphite (HOPG) were held stationary during the simulation and modeled as Lennard−Jones (LJ) spheres. The LJ parameters to describe carbon−carbon interactions were those of Chang and Steele.[69] One SDS surfactant is composed of one hydrophobic tail of 12 carbon atoms (1 CH_3 and 11 CH_2 groups) and one hydrophilic head of chemical composition SO_4. Following Berkowitz and co-workers,[56] who successfully simulated SDS surfactants at a number of fluid−fluid interfaces, the CH_n− groups in SDS were modeled as united-atom LJ groups. Bond lengths and bond angles were constrained by harmonic potentials. The CH_n−CH_n bond length is constrained through the harmonic potential

$$E_{\text{bond}} = K_b(r - r_O)^2 \tag{1}$$

In eq 1 E_{bond} is the potential energy associated with the bond stretching and contraction, K_b is the elastic constant of the bond, r_O is the equilibrium distance between the bonded atoms, and r is the instantaneous distance between them.

All the angles in one surfactant are constrained by the harmonic potential

$$E_{\text{ang}} = K_\theta(\theta - \theta_O)^2 \tag{2}$$

In eq 2 E_{ang} is the potential energy associated with the angle bending, K_θ is the force constant, θ_O is the equilibrium angle, and θ is the instantaneous angle.

Dihedral angles are constrained through the Ryckeart and Bellemans potential[70] given by

$$E_{\text{dihedral}} = \sum_{k=0}^{5} c_k \cos^k(\phi) \tag{3}$$

In eq 3 c_k are the energy constants, φ is the dihedral angle, and E_{dihedral} is the potential energy. The dihedral angles along the backbone of surfactant (CH_n−CH_2−CH_2−CH_2, CH_2−CH_2−CH_2−O*, CH_2−CH_2−O*−S, and CH_2−O*−S−O) were constrained using the parameters shown in Table 1. The head group in each surfactant molecule was explicitly modeled. Sulfur and oxygen atoms in the head group are described as LJ spheres which bear partial charges. The S−O and CH_2−O* bonds are constrained through the harmonic potential expressed in eq 1 with appropriate values for the constants K_b and r_O. The O−S−O and CH_2−O*−S angles are constrained through the angular potential of eq 2, with the appropriate choice of constants.

Sodium ions are modeled following the model of Schweighofer et al.[56] Chlorine atoms, when present, are modeled as described by Cummings and co-workers.[71] Cesium ions, used to study the effect of counterion size on the surface aggregates, were described following Smith and Dang[72] but without polarizability, for consistency with the other potentials used here. LJ interaction parameters for unlike atom pairs were computed from those of like pairs using Lorentz−Berthelot mixing rules. In Table 1 we report all values for the like-pairs parameters used in our simulations.

As mentioned above, all-atom models are too computationally expensive to study the spontaneous formation of micelles at surfactant concentrations at or above the bulk CMC. Bruce et al.,[66] using the model implemented in the present work, studied the morphological properties of one micelle composed of 60 SDS molecules in a system correspondent to a SDS concentration of 0.4 M, but the micelle was prepared as input for the simulation. Gao et al.[73] introduced a simplified model for both SDS and water that allowed them to study the spontaneous formation of micelles from an aqueous solution containing SDS molecules. The SDS concentrations considered were between 0.4 and 1.1 M (well above the bulk SDS CMC). The micelles obtained were rod-like, in qualitative agreement with experimental observation. Although it is not clear whether or not these SDS models predict the bulk CMC concentration in water, the studies just summarized suggest that they are adequate to study the morphology of surfactant aggregates formed at concentrations above the bulk CMC. Because we are interested in capturing atomic-level details that are probably due to formation of hydrogen bonds and salt bridges between interfacial water molecules, surfactant heads, and counterions, we implemented the all-atom model of Berkowitz and co-workers rather than the simplified version of Gao et al. The correct implementation of the model was validated by comparing the average hydration number of head groups at the water−vapor interface with

TABLE 1: Parameters Used To Implement the Force Fields Discussed in Eqs 1−3[a]

atoms (or groups)	σ (Angstrom)	ϵ (kcal/mol)	q (e)
CH_3	3.905	0.175000	0.0000
CH_2	3.905	0.118000	0.0000
CH_2 (in CH_2-O-S)	3.905	0.118000	0.1370
S	3.550	0.250000	1.2840
O* (in CH_2-O-S)	3.000	0.170000	−0.459 0
O (in SO_3)	3.150	0.200000	−0.654 0
H (in H_2O)	0.000	0.000000	0.4238
O (in H_2O)	3.166	0.155402	−0.847 6
C	3.400	0.055700	0.0000
Na^+	2.275	0.115300	+1.000
Cs^+	3.831	0.10000	+1.000
Cl^-	4.401	0.10000	−1.000

bond	K_b (kcal mol^{-1} Å^{-2})	r_o (Angstroms)
CH_3-CH_2	620.000	1.530
CH_2-CH_2	620.000	1.530
CH_2-O^*	600.000	1.420
O^*-S	600.000	1.580
O−S	900.000	1.460

angle	K_θ (kcal mol^{-1} rad^{-2})	Θ_O(deg)
$CH_3-CH_2-CH_2$	124.300	111.000
$CH_2-CH_2-CH_2$	124.300	111.000
$CH_2-CH_2-O^*$	124.300	109.500
CH_2-O^*-S	124.300	112.600
O^*-S-O	102.000	102.600
O−S−O	102.000	115.400

dihedral	C_0 (kcal/mol)	C_1	C_2	C_3	C_4	C_5
$CH_n-CH_2-CH_2-CH_2$	2.2176	2.905	−3.136	−0.731	6.271	−7.527
$CH_2-CH_2-CH_2-O^*$	2.2176	2.905	−3.136	−0.731	6.271	−7.527
$CH_2-CH_2-O^*-S$	2.2176	2.905	−3.136	−0.731	6.271	−7.527
CH_2-O^*-S-O	2.2176	2.905	−3.136	−0.731	6.271	−7.527

[a] O* is the oxygen atom that bridges the CH_2 group and the S atom in SDS surfactants.

neutron-scattering experimental data.[74] The hydration number from our simulations is 8.67, obtained by integrating the sulfur−oxygen (water) radial distribution function up to the first local minima (located at ∼0.55 nm from the sulfur atom). The experimental hydration number is 7 ± 1.[74] We also reproduced the density profiles at the water interface for water, head groups, and tails obtained from MD simulation by Schweighofer et al.[56]

The simulation package LAMMPS[75] was employed to integrate the equations of motion. In our simulations we maintained the number of particles (N), the simulation box volume (V), and the temperature (T) constant. In all simulations the time step was 2 fs. The Nose−Hoover thermostat with velocity Verlet algorithm was implemented with a relaxation time constant of 100 fs.[75] Dispersive attractions and repulsive interactions were treated with an inner cutoff of 0.8 nm and outer cutoff of 1.0 nm. Long-range electrostatic interactions were treated using the Ewald summation method.[75] Bond lengths and angles in water were maintained fixed using the SHAKE algorithm.

Simulations were initialized in a system consisting of two graphite slabs separated by a distance of 6.5 nm. Each graphite slab is composed of three carbon layers, separated by 0.335 nm from each other. The X and Y dimensions of the simulation box are 3.94 and 2.56 nm, respectively. To reach the desired surface area per head group of 0.40 nm^2 we placed 25 SDS surfactants on each graphite slab. In the initial arrangement the SDS surfactants were in the all-trans configuration and perpendicular to the surface. One positively charged sodium counterion was placed at a distance of 0.5 nm from each surfactant head. Sufficient water molecules (1260) were then inserted to reach the desired density (∼1 g/cc) within the simulation box. The initial configuration is shown in Figure 1. Periodic boundary conditions were implemented in three dimensions. To decrease unrealistic interactions between mirror images in the Z direction, 12.1 nm of empty space was placed after the three layers of graphite in the Z direction. Thus, the simulation box was of size $3.94 \times 2.56 \times 20.00$ nm^3. The simulations were initiated by conducting NVT runs at 600 K for 1 ns to ensure that the results were not affected by the initial configuration. The system was then instantaneously brought to 300 K, and the simulations were continued in the NVT ensemble for an additional 2 ns. To further ensure that the results were independent of the initial simulation setup, all sodium counterions were dragged 2 nm away from the head groups in the Z direction. NVT simulations were then conducted for 12 ns. Even though the system energy reached a plateau after ∼1 ns, we only used the molecular trajectories of the last 2 ns to obtain the results presented here.

We performed a number of simulations by varying the distance H between the graphite slabs. To initiate these simulations we used the final configuration obtained from the simulation conducted at $H = 6.5$ nm and removed (or inserted) the necessary amount of water from (or in) the central region of the simulation box.

We computed distribution functions, mean square displacements (MSD), and population distributions to characterize and analyze the results. The distribution function was computed using the following expression[76]

$$Df(r) = \frac{(n_{his}(b)/N \times \tau_{run})}{\frac{4}{3}\pi[(r+\delta r)^3 - r^3]} \quad (4)$$

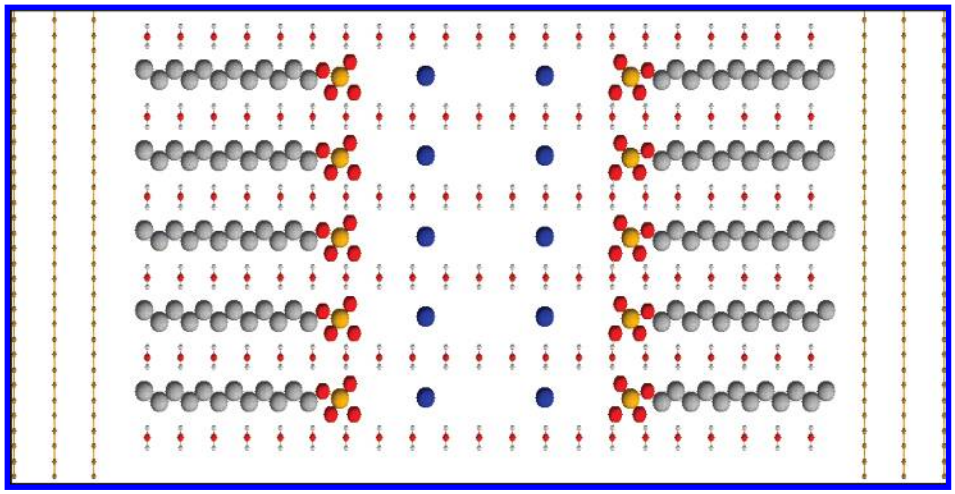

Figure 1. Side view of the initial configuration of SDS at the graphite−water interface. CH_n− groups that belong to the surfactant tails, sulfur, oxygen, and sodium counterions are shown as gray, orange, red, and blue spheres, respectively. Water is represented by small red and white spheres (oxygen and hydrogen atoms, respectively). The graphite surfaces are separated by $H = 6.5$ nm. Graphite atoms are depicted as yellow spheres.

where $n_{his}(b)$ represents the number of elements in the bth histogram, N is the number of particles considered, τ_{run} is the number of output steps recorded during the simulation, r is the center-to-center distance between the atoms, and δr is the width of each histogram bin. In computing distribution functions we do not divide the local density of particles by the average density of the particles within the box. This allowed us to compare the distribution functions in different simulations, irrespectively of the volume of the simulation box.

The MSD, a function of time, is defined by the expression[76]

$$\mathrm{MSD}(t) = \langle |r_i(t) - r_i(0)|^2 \rangle \tag{5}$$

where $r_i(t)$ is the position vector of particle at time t and $r_i(0)$ is the initial position vector of the particle. Angular brackets indicate ensemble averages. The MSD yields the distance traveled by a particle during the time interval considered.

The population distribution of surfactant lengths is defined by the following equation

$$P(r) = (n_{his}(b)/N \times \tau_{run}) \tag{6}$$

where $n_{his}(b)$ represents the number of elements in the bth histogram and N and τ_{run} are defined as in eq 4.

3. Results and Discussion

(a) Frontal Confinement. We provide here the results from simulations conducted at graphite−graphite separation distances $H = 4.055$, 4.50, 6.50, 8.00, 10.00, 12.00, and 14.00 nm. We report the distribution function between sodium and sulfur atoms in Figure 2. The statistical error is ∼5%. Although the curves shown in Figure 2 are similar to each other, they present interesting differences as a function of the graphite−graphite separation distance H. A sharp peak is evident in all S−Na distribution functions at a distance $r \approx 0.35$ nm. This well-pronounced peak corresponds to the association of the counterions to the surfactant heads. We notice that this peak is present for all graphite−graphite separations considered. However, the peak intensity for the distribution function obtained at $H = 4.05$ nm is larger when compared to that obtained when $H = 4.5$ nm. It is possible that when the graphite−graphite distance is reduced from $H = 4.5$ nm to $H = 4.05$ nm the surface aggregates adsorbed on the two opposing surfaces interact with each other. The fact that the $Df_{S-Na}(r)$ peak at 0.35 nm increases

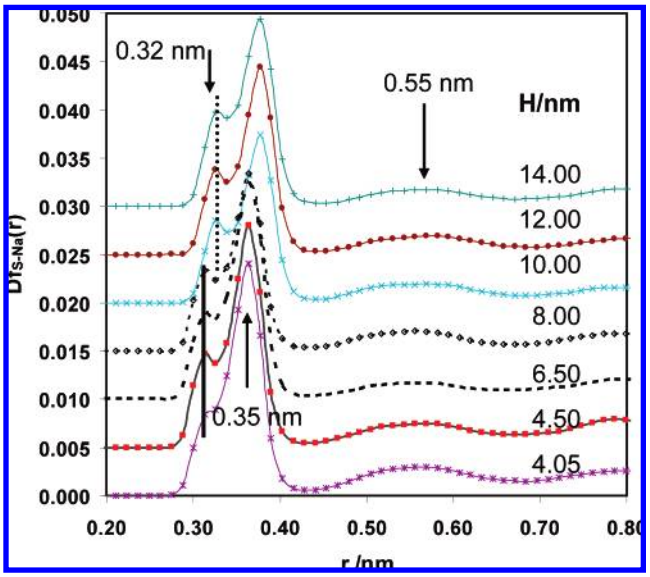

Figure 2. Distribution function between sulfur and sodium for the simulations conducted at different graphite−graphite separations H. From bottom to top the different lines are for $H = 4.05$, 4.5, 6.5, 8.0, 10.0, 12.0, and 14.0 nm. The vertical lines and arrows indicate the observed peaks. Two vertical lines (continuous and dotted) highlight the shift of the ∼0.32 nm peak to longer S−Na distances when H increases above 8.0 nm. Individual plots are shifted 0.005 units along the Y axis to ease visualization.

suggests that Na^+ may form ion bridges between the surfactant heads which belong to the two opposing surfaces. When the graphite−graphite separation distance H increases from 4.05 to 6.50 nm, the intensity of the $Df_{S-Na}(r)$ peak at 0.35 nm decreases monotonically. It is interesting to note that the peak at 0.35 nm obtained at $H = 6.5$ nm and that obtained at $H = 8.0$ nm are indistinguishable from each other. As H further increases to values above 8.0 nm the peak intensity does not change but the peak location shifts to larger S−Na separations. At S−Na separations larger than 0.40 nm we observe smooth oscillatory behavior of the distribution function which does not indicate significant structuring between the surfactant heads and the counterions. However, we point out that the second weak peak in the distribution function, located at $r = 0.55$ nm, becomes slightly more intense as the graphite−graphite separation decreases. This behavior is different from what is observed for SDS surfactant micelles in aqueous solution, in which case

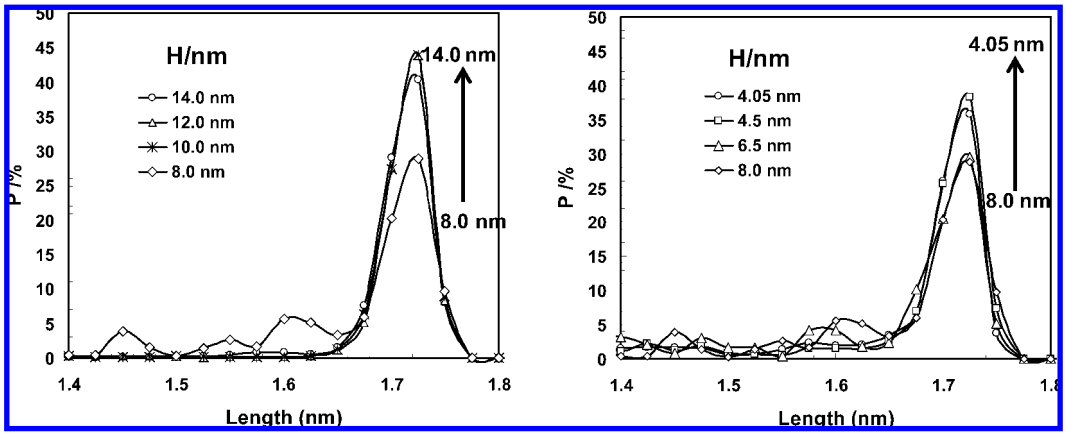

Figure 3. Population distribution of surfactant lengths. The different curves depict the distribution of surfactant lengths in the simulations conducted at different graphite−graphite separations *H*.

a significant second peak for the S−Na radial distribution function is observed at ∼0.43 nm, which corresponds to the second shell of counterions around the surfactant heads.[66] Interestingly, while in the case of micelles 50% of the counterions distribute between the first and second shell around the surfactant heads,[66] our results indicate that in the case of SDS aggregates on graphite about 75% of the Na^+ counterions accumulate within the first solvation shell. This result is in qualitative agreement with experimental data obtained by Bitting and Harwell for Li^+, Na^+, K^+, and Cs^+ salts of dodecyl sulfate aggregates on alumina, which suggest that 'apparent' counterion−surfactant head binding on surface aggregates can be up to 85−95%, depending on solution conditions.[77] We also detect a small peak at short separations (0.32 nm). The peak is well pronounced when *H* is larger than 4.5 nm, and it becomes but a shoulder at $H = 4.05$ nm. At *H* greater than 8.0 nm this peak shifts from ∼0.32 to ∼0.34 nm, as indicated in Figure 2 by the distance between the continuous and dotted vertical lines. This small peak may be due to the presence of the Na^+ sandwiched between two next-neighbor SDS surfactant heads, suggesting the possibility of counterion bridging, as documented in the next section.

To investigate the packing of SDS molecules within the surface aggregates we calculated sulfur−sulfur distribution functions. A hemi-cylindrical arrangement should yield a distribution function characterized by broad peaks located at regular intervals. Our results (not shown for brevity) indicate that the head groups are associated with each other only for distances lower than 0.8 nm. The first peak, which does not change as *H* varies, is observed at S−S distances of 0.45 nm, and a second broad peak, which becomes less intense as *H* increases, is observed at a S−S distance of ∼0.7 nm. The second peak suggests some degree of ordering between the head groups, although it does not necessarily imply formation of any specific supramolecular structure (e.g., hemi-cylinders).

The results discussed so far suggest that the properties of the SDS surface aggregates depend on the graphite−graphite separation. It is possible that when *H* approaches twice the thickness of the surface aggregate effective forces act between the aggregates, thus affecting the equilibrium structure of the aggregates. To test this hypothesis we calculated the population distribution of the surfactant lengths as a function of *H*. The surfactant length is calculated as the distance between the CH_3 group in the surfactant tail and the farthest oxygen atom in the surfactant head. The results, whose statistical error is less than 5%, are shown in Figure 3. In the right panel we display the results obtained for graphite−graphite separations *H* ranging from 4.05 to 8.00 nm. We notice that the pronounced peak for a surfactant length of ∼1.7 nm increases significantly as *H* decreases. It is particularly interesting to note that the data sets obtained for $H = 6.50$ and 8.00 nm almost coincide. In the left panel of Figure 3 we display the results obtained when *H* increases from 8.0 to 14.0 nm. In contrast to what is observed at smaller *H*, we notice that the percentage of surfactant molecules of length 1.7 nm increases as *H* increases from 8.0 to 10.0 nm and larger separations. These results suggest that as the graphite surfaces approach from $H = 14.0$ nm to $H = 6.5$−8.0 nm the surfactant molecules are compressed, as evidenced by the decreasing probability of observing surfactants of length 1.7 nm, possibly indicating an effective repulsion between the surfactant aggregates adsorbed on the two opposing graphite surfaces. As the graphite surfaces further approach, the surfactants begin to stretch, possibly indicating an attraction between the surfactant aggregates adsorbed on the two opposing surfaces. We point out that during our simulations we never observed desorption of the surfactant molecules from one surface followed by adsorption onto the opposing surface, as could have been expected based on the SCF calculations of Leermakers and coworkers.[26] It is possible that such phenomena can be observed for longer simulations, which are at present prohibitive.

The results discussed until now suggest that when the graphite slabs are closer than 6.5−8.0 nm there may be a significant attraction between the surfactant aggregates on the two surfaces. This is in qualitative agreement with the observations of Wanless and Ducker,[22] who reported that AFM tips 'feel' the presence of SDS surface aggregates on graphite when they are at a distance of ∼10 nm or less from the solid surface. On the basis of our results, in order to study the behavior of independent SDS aggregates at the water−graphite interface *H* should be at least greater than 8.0 nm, although this distance may vary depending upon the type of head group, surfactant length, and ionic strength of the system. To further test our hypothesis, we focus on the diffusion of the surfactant aggregates on the two opposing surfaces. In the presence of a strong aggregate−aggregate attraction (as well as repulsion), we expect that the aggregates on the opposing surfaces move in a coordinated fashion. If the two aggregates are not influenced by the presence of each other, then the surface displacement of each should be independent from that of the other. We calculated the mean square displacement (MSD) for the sulfur atom in the surfactant head group. We report the results in Figure 4. In the case when graphite surfaces are separated by 4.05 nm (left panel), we observe that the surface aggregates on both surfaces move in a highly coordinated manner along both the *X* and *Y* directions.

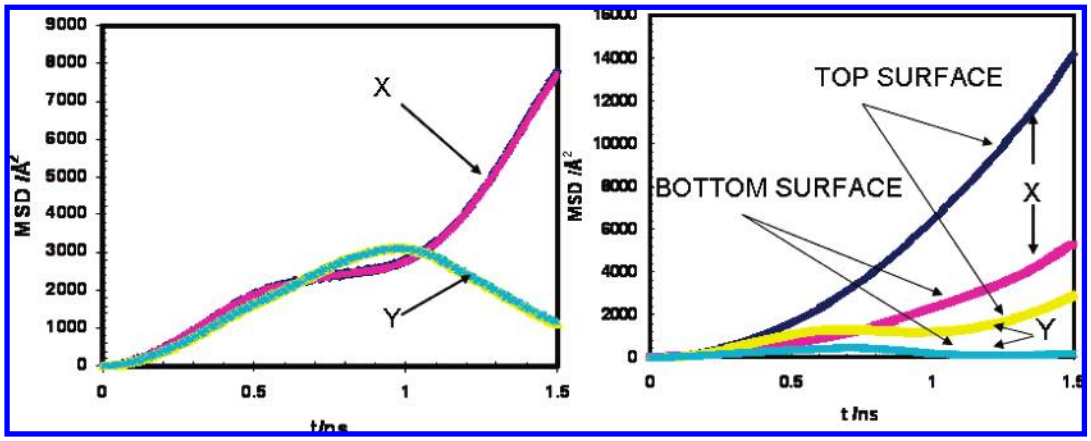

Figure 4. (Left) MSD vs time for sulfur atoms within the surface aggregate when graphite−graphite distance $H = 4.05$ nm. (Right) MSD vs time for sulfur atoms within the surface aggregate when $H = 14.00$ nm. Blue and pink lines are for MSD along the X direction for top and bottom surface aggregates, respectively; yellow and green lines are for MSD data along the Y direction for top and bottom surface aggregates, respectively. Blue and pink lines, as well as yellow and green lines, are indistinguishable in the left panel.

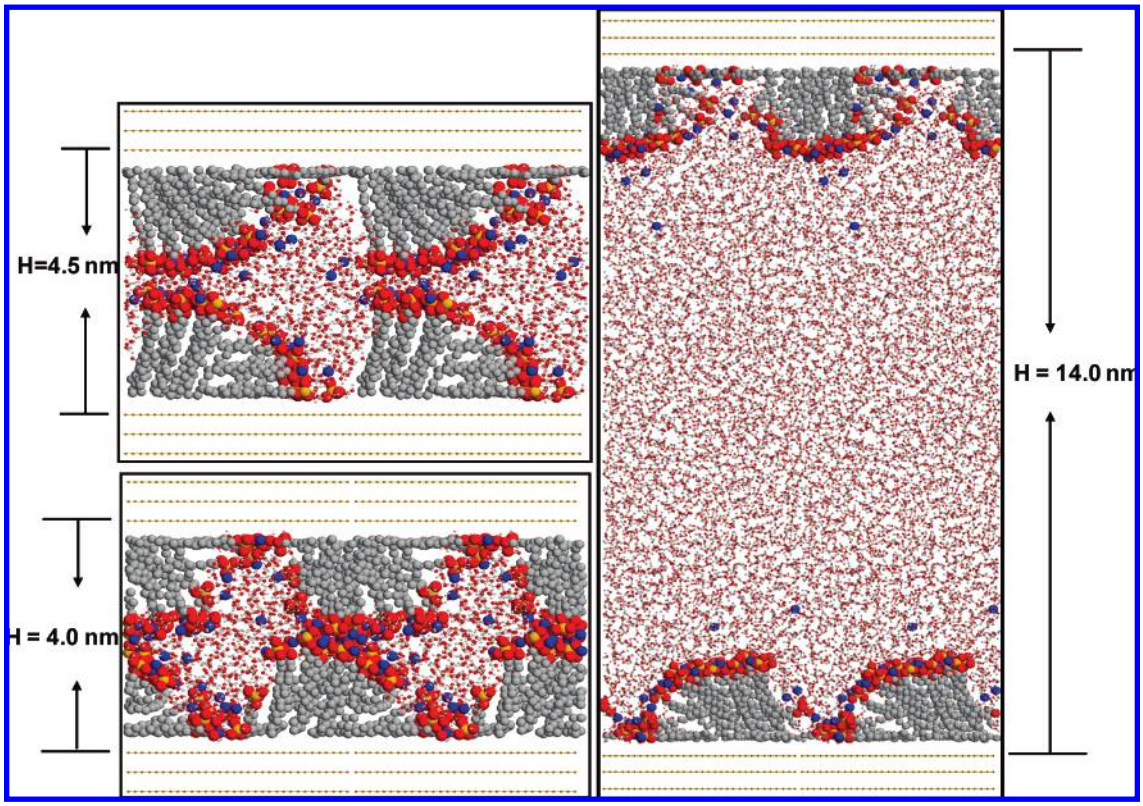

Figure 5. Side view of representative simulation snapshots obtained at various graphite−graphite separations H. CH_n− groups in surfactant tails, sulfur, oxygen, and sodium counterions are shown as gray, orange, red, and blue spheres, respectively. Water is represented by small red and white dots (oxygen and hydrogen atoms, respectively). Graphite atoms are shown as yellow spheres. The simulation box is replicated twice along the X direction for visualization purposes.

In fact, the MSD calculated for the surfactant aggregate on the top surface is not distinguishable from that calculated for the surface aggregate on the bottom surface, confirming our hypothesis of strong attraction between the surface aggregates. On the other hand, the MSD data obtained at $H = 14.0$ nm (right panel) show significant deviation between the results obtained for the surfactants aggregates adsorbed on top and bottom surfaces, respectively. This uncoordinated behavior suggests that the surface aggregates on each surface are not influencing each other. Our complete set of results (not shown for brevity) indicate that the diffusion of the surface aggregates on the two opposing surfaces is somewhat correlated even at $H = 4.5$ nm. It is interesting to note, from the results in Figure 4, that the MSD along the Y direction is oscillatory. The amplitude of these oscillations along the hemi-cylinders axis is ∼1 order of magnitude less than the MSD along the X direction measured in ∼1.5 ns of simulation. We point out that the MSD, even that along the X direction, is not sufficiently large to yield accurate estimates for self-diffusion coefficients; thus, we do not attempt such calculations.

(b) Equilibrium Structure. We now discuss the morphological details of SDS surface aggregates. In Figure 5 we show the equilibrium structure of surface aggregates for various graphite−graphite distances (H) by means of representative simulation snapshots. We report surface aggregates obtained for $H = 4.05$, 4.50, and 14.0 nm. On the basis of the results discussed above,

at $H = 4.05$ and 4.50 nm the surface aggregates strongly feel the presence of each other, but at $H = 14.0$ nm the surface aggregates are expected to be noninteracting.

All the snapshots shown in Figure 5, as well as all the others not shown for brevity, indicate that SDS surfactants adsorbed on the graphite−water interface yield hemi-cylindrical aggregates at the conditions considered here. More interestingly, we always find regions within the SDS aggregates in which the hydrophobic surfactant tails are exposed to water. It is evident from the snapshots of Figure 5 that this is due to the fact that head groups closely pack with each other and with sodium counterions.

Although the qualitative morphology of the surface aggregates does not change as H decreases, we note in Figure 5 that the surfactant aggregates which are adsorbed on the opposing surfaces interact strongly with each other. The surface aggregates on the opposing surfaces resemble each other when $H = 4.05$ nm. The head groups of the surface aggregate are found very close to each other rather than distant as it would be expected because of electrostatic repulsions between like-charged head groups. A few Na^+ counterions are found sandwiched between surfactants which belong to the aggregates of the two opposing surfaces. This "counterion condensation" results in an effective attraction between the head groups of opposing surface aggregates. In the snapshot obtained for $H = 4.5$ nm the surface aggregates from opposing surfaces seem to stretch in an attempt to touch each other. This structure, along with the larger population distribution observed for surfactants with length 1.7 nm shown in Figure 3, suggests that attractive forces act between the surface aggregates adsorbed on the opposing graphite surfaces. We did not attempt to quantify these forces. When $H = 14.0$ nm the surface aggregates on the opposing surfaces are not identical, and the surface aggregate on the bottom surface looks similar to those observed when $H = 4.05$ and 4.5 nm (note that these snapshots were obtained after at least 10 ns of simulation time). We also notice that morphological distortions from perfect hemi-cylindrical structure, which are always observed during our simulations, are more pronounced when the two graphite surfaces are at small distance from each other, probably because under those circumstances the surfactant aggregates on the two opposing surfaces strongly attract each other. A complete understanding of the molecular origin for this phenomenon could allow us to tailor the self-assembly of amphiphilic molecules of practical interest.

Because of periodic boundary conditions and confinement effects it is possible that the results just discussed are affected by the simulation box size along the X direction (which constrains the distance between two adjacent hemi-cylinders) and of the density of water within the simulation box (which determines the pressure of the system). To assess the reliability of our calculations we performed additional simulations in two representative cases. In the first case study we addressed the effect of box size on the structure and morphology of SDS aggregates. The initial simulation box was replicated twice along the X direction, and the box was further 'grown' in that direction until the X size was 8.36 nm. One of the two opposing graphite surfaces and the surface aggregates on that surface were removed. The resultant system contained 3455 water molecules, 50 SDS, and 50 Na^+ ions. The available surface area per surfactant molecule was 0.42 nm^2. Because the Y and Z dimensions of the simulation box were maintained equal to those discussed in section 2, the new simulated system now exhibits one vacuum−water interface. As customary, periodic boundary conditions were implemented in the three directions.

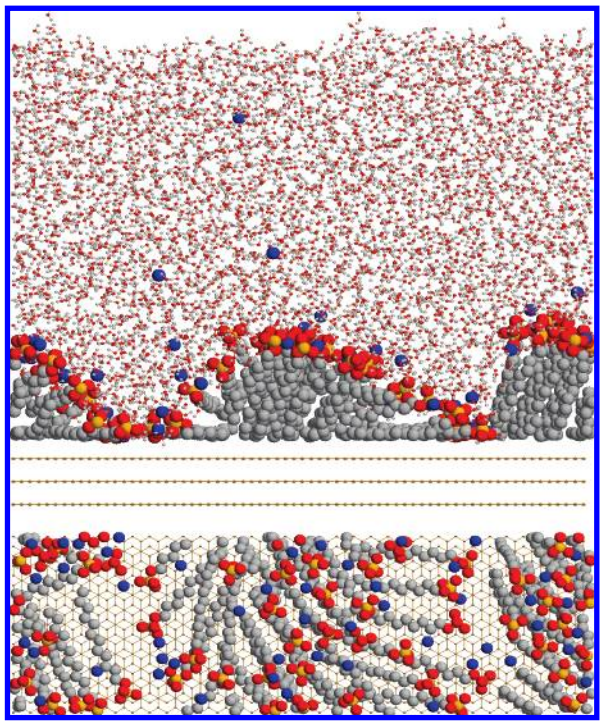

Figure 6. Lateral (top) and top view (bottom) of the simulation snapshot obtained after 10 ns in a box of size $X = 8.36$ and $Y = 2.56$ nm. The lateral view is qualitatively identical to that obtained in the simulation box of size $X = 3.94$ nm (see Figure 5). The top view (from which water molecules are deleted) provides details on the morphological arrangement of the aggregates.

After 10 ns of simulation time, the SDS molecules yield two hemi-cylindrical aggregates, one adjacent to the other. As can be seen from the final simulation snapshot shown in Figure 6, the morphology of each aggregate was similar to the one obtained in the original simulation box (Figure 5). Further, density profiles and distribution functions computed from both simulations (Figures 5 and 6) were not distinguishable within computational accuracy. These comparisons suggest that the simulation box of $X = 3.94$ nm is sufficiently wide to obtain reliable morphological information. The experimental AFM results of Wanless and Ducker[22] show that the distance between two adjacent SDS hemi-cylindrical aggregates at the graphite−water interface decreases as the SDS surface coverage increases. It ranges from ∼7.0 nm at 2 mM SDS bulk concentration to ∼5.2 nm at 100 mM. Although our results, dictated in part by the simulation box X dimension, are in reasonable agreement with experiments, our simulation protocol is not adequate to predict the equilibrium aggregate−aggregate separation as a function of surface coverage. Much larger and at present untractable systems are required for these purposes.

The second case study was conducted by implementing an *NPT* (constant number of particles, pressure, and temperature) algorithm in which one of the two opposing graphite surfaces, along with the surface aggregate on that surface, was removed. Because of periodic boundary conditions in the Z direction, the vacuum−water interface of Figure 6 is replaced by a graphite−water interface. To maintain the pressure constant at atmospheric conditions the simulation box height (Z direction) was allowed to fluctuate. After 15 ns, the simulation yields similar structural and morphological details as those observed when $H = 8.0$ nm in the simulations described above. On the basis of the results obtained in the two latter case studies and how they favorably compare to the results obtained within the original simulation box, we are confident that within the accuracy of the force fields

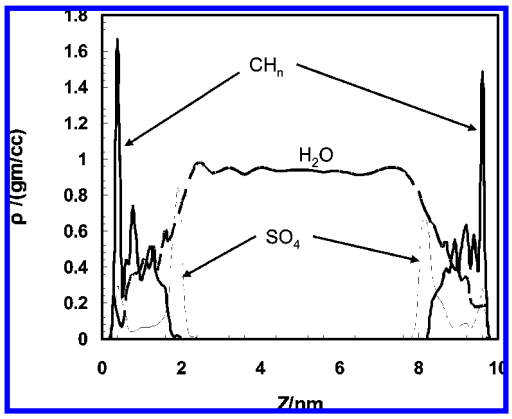

Figure 7. Density profiles for surfactant tails (continuous gray line), surfactant head groups (broken gray line), and water molecules (broken black line) as a function of the distance from the graphite surface.

implemented in this work the morphological results shown in Figure 5 are representative of the self-association of SDS surfactants at the graphite−water interface at room conditions. The results discussed in the remainder of the manuscript are obtained in the small simulation box.

Density profiles across the simulation box obtained from the equilibrium surface aggregates are reported in Figure 7. We include the density profiles of surfactant tail groups, head groups, and water molecules along the *Z* direction when the distance between the graphite surfaces is 10.0 nm, i.e., when the interactions between surfactant aggregates on opposing surfaces are negligible. We did not observe any significant difference in density profiles calculated for surfactant head groups and tails among all the simulations performed for graphite−graphite separations larger than 8.0 nm. Concerning the density profile of head groups (broken gray line) we observe a clear, albeit small, peak at ∼0.4 nm. This result is quite surprising (hydrophilic heads are not expected to lie close to the graphite surface) but is due to the parallel orientation of a few surfactant molecules on the surface, as suggested by the peaks in the results for the tail groups density profiles. The number of SDS molecules that lie completely on the graphite surface are computed by averaging the surfactants that are always within less than 0.6 nm from the graphite surface. We found that always 20−30% of the surfactant molecules lie parallel to graphite. From the results of Wanless and Ducker[22] we expect that seven surfactants are present in each cross section of one SDS hemi-cylinder, out of which at least two should lie parallel to graphite (i.e., ∼28%). The head group density is the highest at ∼1.84 nm from the graphite surfaces, a value which corresponds to the thickness of the aggregate structure. This result is in reasonable agreement with the AFM experiments of Wanless and Ducker, which indicate an aggregate thickness of 1.7 ± 0.5 nm.[22] Our result is also in agreement with the recent MD simulations of Dominguez.[65] One would expect the density profile of water to gradually decrease from one in the center of the simulation box to zero at the hydrophobic graphite surface. However, as we can notice in Figure 7 (broken black line) the results for the water density profiles are more interesting. For example, we notice the presence of a small peak at about 0.4 nm from the graphite surfaces, indicating the presence of water molecules near the graphite surface. This unexpected result is due to the presence of few surfactant head groups on the graphite surface, which in turn attract water molecules to the surface. In Figure 7 we observe a very sharp intense peak at 0.4 nm from either graphite surface for the density profile of surfactant tail groups (continuous gray line). This peak suggests that a few surfactant tails are adsorbed completely parallel to the surface. We also notice that the density profile for tail groups shows several peaks at distances larger than ∼1.0 nm from the graphite surface, indicating the presence of not regularly adsorbed tails. This suggests formation of structures in which the tail groups are neither completely parallel to the graphite surface nor perpendicular to it.

In our simulations the SDS molecules do not yield perfect hemi-cylindrical structures. Perfect hemi-cylinders are shown schematically in Figure 8a. In such structures it is possible to define the angle α formed between the *X* direction of the simulation box and the vector obtained by connecting the first and last methyl group in one SDS molecule (see schematic in Figure 8b). When $\alpha = 0°$ or 180°, the surfactant is parallel to the *X* surface direction. When $\alpha \approx 90°$, the surfactant is perpendicular to the surface. Surfactant organized in perfect hemi-cylinders should yield symmetric distributions of angles α with peaks at 0°, 90°, and 180°. Instead, we see (black continuous line in Figure 8c) that SDS surfactants at the graphite−water interface are either perpendicular or parallel to the surface, but the angles in between are not often sampled. In agreement with this observation, an enlargement of the density profiles for the surfactant head groups (black continuous line in Figure 8d) shows that most of the surfactant heads are either located next to the surface or located at ∼1.7−2.0 nm from it.

Both the simulation snapshots shown in Figure 5 and the head group density profiles shown in Figures 7 and 8d suggest that the head groups for SDS surfactants at graphite−water interfaces are not uniformly distributed. Instead, we find that the head groups form few dense patches within the surface aggregate, which cause some of the surfactant tails to be exposed to the aqueous environment. To further highlight this phenomenon we present in Figure 9 the top view of one simulation snapshot obtained for SDS aggregates at the graphite−water interface.

The presence of sporadic dense patches formed by counterions and head groups is apparent from Figure 9 (highlighted by the yellow circle). Because of the presence of these dense patches, some of the hydrophobic surfactant tails remain exposed to the aqueous environment, as evidenced by the black circle in Figure 9. The dense patches of surfactant heads are also the reason for the noticeable contrast between the snapshots shown in Figures 5 and 6 and the schematic representation proposed in Figure 8a, i.e., the surfactant head groups completely shield the hydrophobic tails from water in Figure 8a but do not do so in Figures 5 and 6.

To assess the role played by the counterion condensation in the results shown above, we report an enlargement of one simulation snapshot in Figure 10. This figure allows us to highlight the counterion-bridging phenomenon observed in all surface aggregate structures discussed so far. In Figure 10 the distances between the sodium counterion and the sulfur atom of two adjacent surfactants are at 0.30 and 0.348 nm. These distances give rise to the two peaks observed in the S−Na distribution function, Figure 2. The sodium counterion associates simultaneously with several surfactant heads, neutralizing the charge−charge repulsion expected between the ionic heads and instead inducing an effective attraction. This attraction is strong enough to cause formation of the hydrophilic dense patches discussed in Figures 5 and 9.

On the basis of the discussion relative to Figure 10, we may expect that the morphology of the SDS aggregates at the graphite−water interface is affected by the size of the counterions. Namely, if counterions bigger than Na^+ were considered,

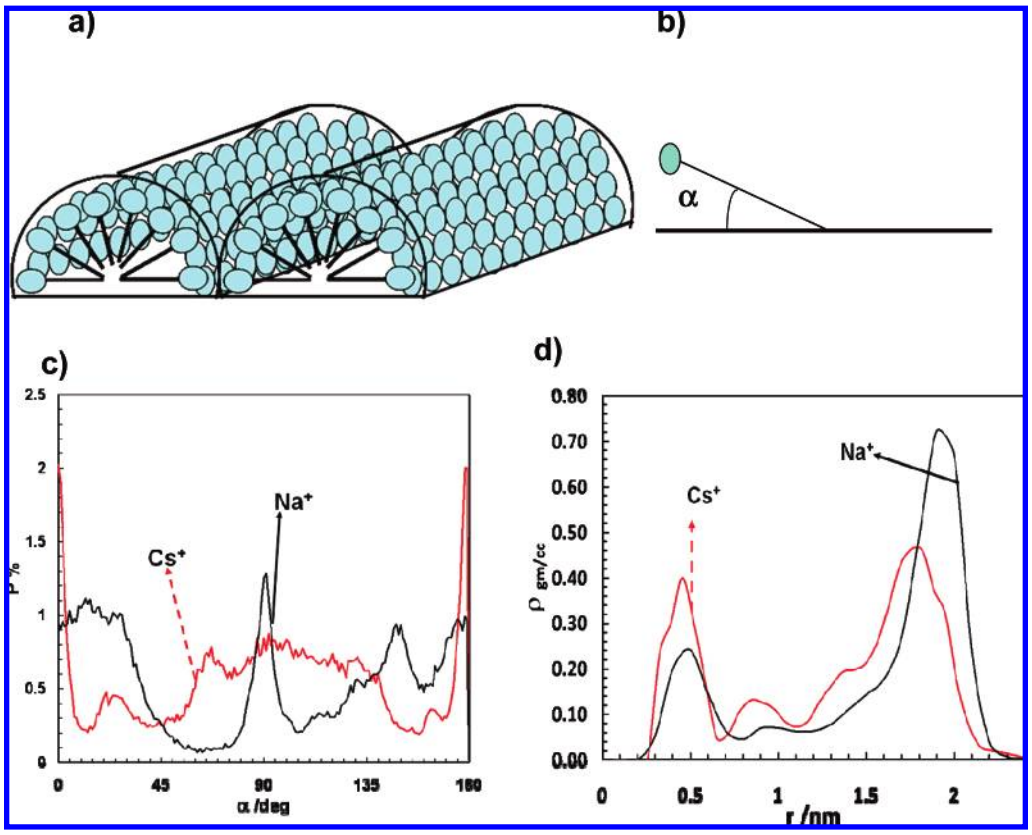

Figure 8. (a) Schematic representation of perfect surfactant hemi-cylindrical aggregates on hydrophobic surfaces. The light blue spheres represent the head groups. In this idealization the surfactant head groups shield the hydrophobic tails from the aqueous solvent. (b) Schematic of the angle α formed between one surfactant molecule and the *X* direction of the simulation box. (c) Population distribution of angle α. (d) Density profiles of surfactant head groups. In panels c and d, black and red lines represent results obtained with Na^+ and Cs^+ counterions, respectively.

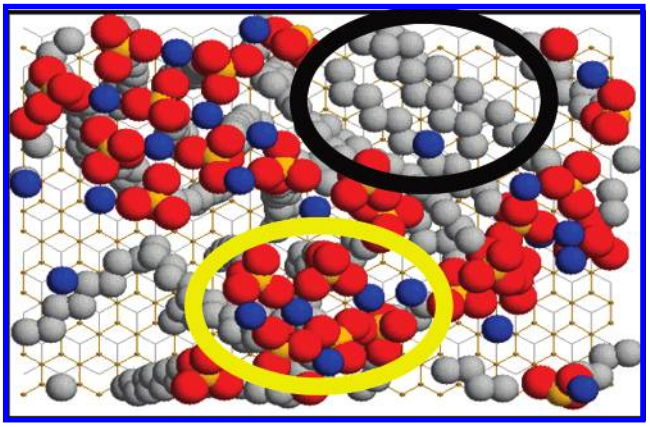

Figure 9. Top view of SDS aggregates formed on graphite surfaces. The color code is the same as that used in Figure 5. The black circle highlights an area in which the hydrophobic surfactant tails are exposed to water. The yellow circle indicates one dense patch composed by head groups and counterions.

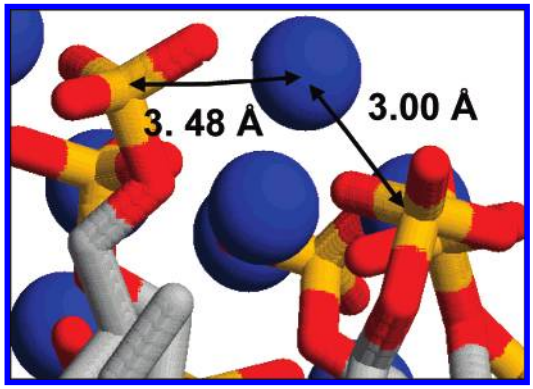

Figure 10. Counterion bridging as observed within the SDS surface aggregate. The color code is the same as that of Figure 5. In the cartoon the atoms are connected using the stick model. The distance between counterion and adjacent head groups is indicated (3.48 and 3.00 Å are the distances from the left and right head groups to the Na^+ counterion, respectively).

the patches of surfactant heads and counterions should become bigger and therefore provide wider shields to the hydrophobic surfactant tails from the aqueous environment. To test this hypothesis we conducted a series of simulations in which the Na^+ counterions were substituted by the much larger Cs^+ ones. In Figure 11 we report the equilibrium simulation snapshot obtained in this latter case. Confirming our hypothesis regarding the importance of counterion-condensation phenomena in the formation of the hemi-cylindrical aggregates of Figure 5 (in which hydrophobic tails are exposed to water), the snapshot shown in Figure 11 indicates that when Cs^+ ions are considered, the surface SDS aggregates become perfect hemi-cylinders in which the hydrophilic heads act as a perfect shield to the hydrophobic tails. The aggregates in Figure 11 were characterized by computing the probability distribution of the angle α (see Figure 8b) and the head group density profile away from the graphite surface. We report the results in Figure 8c and d, respectively, where we directly compare them to those obtained when Na^+ were the counterions. In the case of Cs^+ (red lines) the probability distribution of the angle α shows peaks at 0°, 90°, and 180°, but the angles in between are sampled with some probability, as expected for quasi-perfect hemi-cylindrical aggregates. Further, the density distribution of head groups (red line in Figure 8d) shows a somewhat homogeneous distribution, as expected from the snapshot in Figure 11.

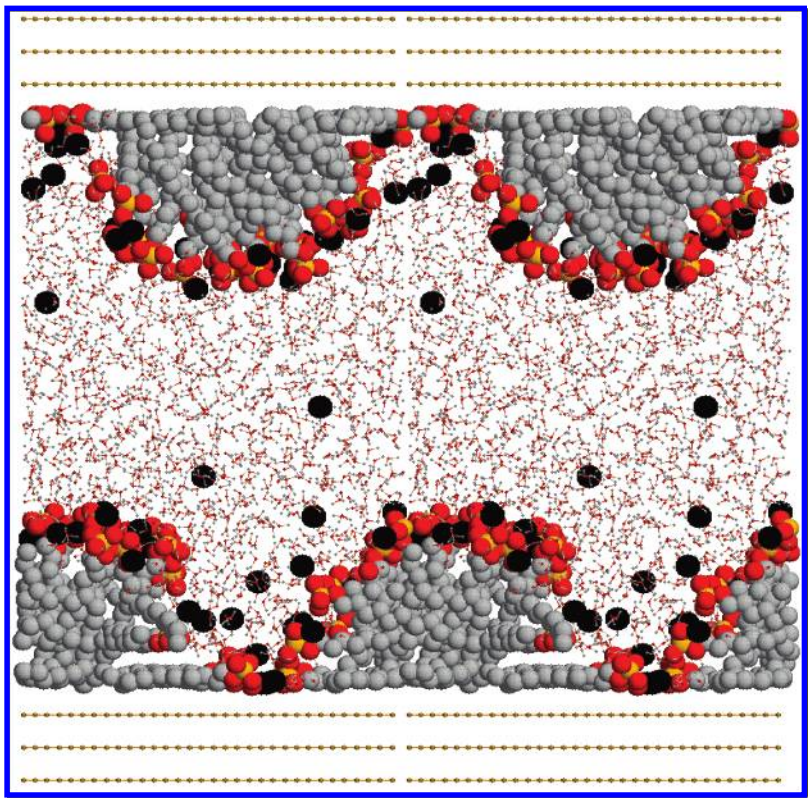

Figure 11. Side view of one representative simulation snapshot obtained when the counterion is cesium rather than sodium at $H = 6.5$ nm. The color code is the same as that used in Figure 5, except for cesium atoms, which are represented by black spheres. The simulation box is replicated twice along the X direction for visualization purposes.

The results discussed so far indicate that the presence of sodium counterions in the vicinity of head groups influences the morphology of the self-assembled aggregates. We studied the MSD of sodium counterions to differentiate their behavior when they are associated with surfactant aggregates compared to when they are in the bulk aqueous solution. The comparison of MSD results of the sulfur atoms (representing head groups) to that of all the counterions present in the simulation box suggests that the surfactant head group and counterion movements are highly correlated but not completely identical. Instead, if we compare the MSD obtained for the sulfur atoms to that of the MSD obtained for only those counterions found within the first shell around the surfactant head groups (within a center-to-center distance of ~0.41 nm), we find identical behavior. These results (not shown for brevity) further indicate that counterions are strongly associated with the head groups. Further, only a few Na^+ or Cs^+ counterions (~25% of the total) are found in the bulk solution during our simulation. The MSD obtained for these ions is larger than that obtained for the counterions found near the surfactant head groups.

(c) Nonionic SDS-Like Surfactants. The manifestation of phenomena such as counterion bridging and condensation in the surface aggregate structure induced us to reexamine the aggregate structure closely and study the driving forces for such aggregation on surfaces using a parametric study. We report in what follows the results of a series of simulations conducted for nonionic SDS-like surfactants. The goal of these simulations is to unveil the physical origin of the results discussed so far. In particular, we are interested in understanding why SDS surfactants form hemi-cylinders at the graphite−water interface and also why some of the hydrophobic tails remain exposed to the aqueous environment. The final configuration from the simulation of SDS at the graphite−water interface in which the graphite surfaces are separated by 6.50 nm was used as the initial configuration for the nonionic SDS-like surfactants. The Coulombic charge of the atoms present in the SDS head group was set to zero, and the hydrophilicity of the head groups was regulated by increasing the interatomic LJ interaction parameters between all head group atoms (which were S and O in the case of SDS) and water. Anionic chlorine atoms were introduced within the simulation box for the purpose of attaining electrical neutrality. Simulations were performed with interatomic interaction parameter set to ϵ_1, $2\epsilon_1$, 2.5 ϵ_1, $3\epsilon_1$, $3.5\epsilon_1$, and $4\epsilon_1$, where ϵ_1 corresponds to the LJ well depth obtained from the Lorentz−Berthelot mixing rules for LJ parameters of the head group atoms and the oxygen atom in water using the values reported in Table 1. Thus, for example, when the simulations were conducted for $4\epsilon_1$, the LJ energy parameter to determine S−O (water) interaction was 0.78842 kcal/mol, whereas the LJ energy parameter for the S−O pair in the simulations conducted for SDS was 0.19710 kcal/mol.

For the weakest head group−water interactions corresponding to the interaction parameter of ϵ_1 we observe multiple layers of the surfactant on the graphite surface (see top left panel in Figure 12). Formation of multiple layers is justified by energetic reasons. Because of the weak attraction between the head group and water, the entire surfactant molecule acts essentially as a hydrophobic chain. Thus, the surfactant molecules partition preferentially at the graphite surface in an effort to minimize the contact with water molecules. The surface aggregate structure depicted on the top right panel of Figure 12 is obtained when the LJ interaction parameter used is $2\epsilon_1$. The increase in the head groups' hydrophilicity is responsible for changing the morphology of the surface aggregates, which now resemble straightened multiple layers. Further increasing the head group−water interaction strength, we observe gradual transition of the surface aggregate structure from multiple layers to 'raising pancakes' obtained for LJ parameters of $3\epsilon_1$ (lower left panel)

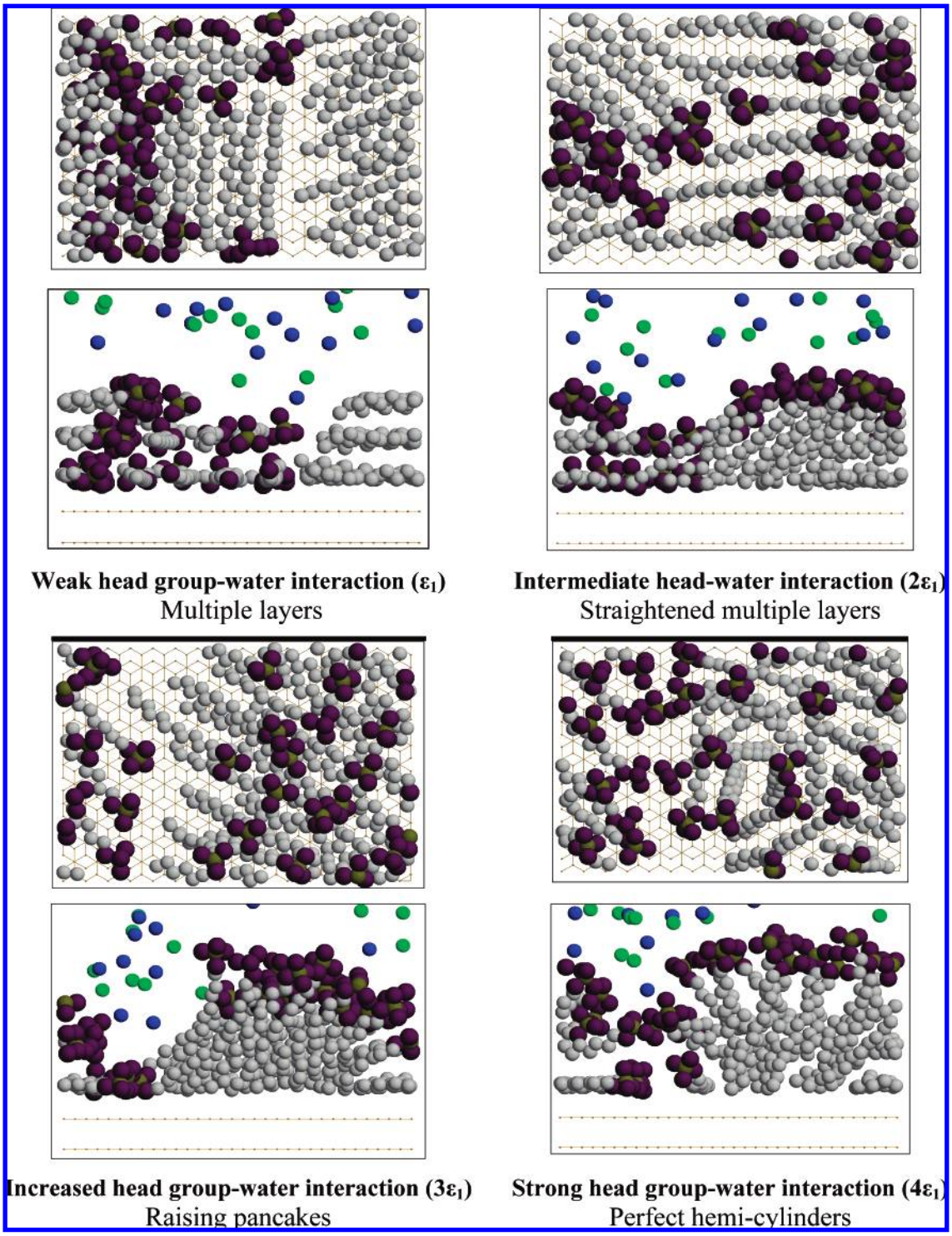

Figure 12. Representative simulation snapshots for nonionic SDS-like surfactants with varying head group−water interactions. In each panel, we provide a top (above) and lateral (bottom) view of the simulation snapshot obtained for nonionic SDS-like surfactants on graphite surface. Carbon, sulfur, oxygen, sodium, and chlorine atoms are shown as gray-, olive green-, maroon-, blue-, and green-colored spheres, respectively.

and to perfect hemi-cylindrical aggregates obtained for LJ parameters of $4\epsilon_1$, as depicted in the lower right panel of Figure 12.

Perfect hemi-cylinders are observed only when strong head group−water van der Waals interactions are considered. In this case the water molecules are strongly attracted to the surfactant heads; thus, the effective area for head groups increases when compared to the simulations of SDS reported above. In the case of SDS surfactant the Coulombic charges present on the head groups introduce hydrophilicity, but the effective surface area per head group decreases due to the counterion-condensation phenomenon illustrated in Figures 9 and 10.

To quantify the differences between the surface aggregates obtained for SDS surfactants in the presence of Na^+ counterions or Cs^+, as opposed to those obtained in the case of nonionic SDS-like surfactants with strong head group−water interactions ($4\ \epsilon_1$), we calculated the S−S distribution function, which is reported in Figure 13. It is evident from Figure 13 that the distribution functions obtained in the three simulations differ in both location and intensity of the peaks. The first peak is

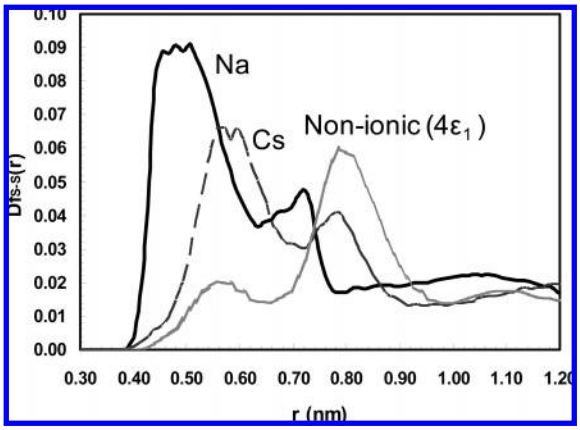

Figure 13. Sulfur−sulfur distribution function. Continuous black line represents the distribution function obtained for the surface aggregate with sodium counterion, dotted black line for cesium counterion, and continuous gray line for nonionic SDS-like with strong head group−water attraction ($4\epsilon_1$).

more intense than the second in the case of SDS surfactants in presence of Na^+ and Cs^+ counterions, while the second peak is more intense than the first in the case of SDS-like nonionic surfactants. The effect of counterion size can be observed from the difference in the location of the first peak when counterions are either sodium or cesium. In fact, the position of the first peak in the presence of sodium counterion is ∼0.45 nm, and it increases to ∼0.56 nm in the presence of cesium counterions, suggesting that the 'effective' size of the surfactant heads depends on the nature of the counterions. When the nonionic SDS-like surfactants are considered, the first peak in the S−S distribution function is not well pronounced, a result that we ascribe to the absence of counterion-condensation phenomena. Because the head groups strongly attract water molecules, not many head groups can be found within a distance of 0.45 nm from a sulfur atom, which corresponds to the location of the first peak. The presence of few surfactants at smaller center-to-center distances results in an intense second peak which appears at center-to-center distances of ∼0.8 nm.

We also computed the number of water molecules present within the first shell of the head groups (referred to as the hydration number) for both ionic and nonionic surfactants. This was done by integrating the sulfur(surfactant head)−oxygen-(water) radial distribution function to its first local minima. The hydration number for SDS at the graphite−water interface in the presence of sodium counterions yields 10.5 water molecules within the first shell. The increase in hydration number for surface aggregates on graphite compared to the air−water interface is due to the curvature of the aggregate on the graphite surface. When the sodium counterions are replaced by cesium ions the hydration number drops to 7.25, indicating that, because of the larger size of Cs^+ compared to Na^+ ions, fewer water molecules can fit near the surfactant heads. The hydration numbers for nonionic SDS-like surfactants strongly depend on the head group−water interaction strength. Our results indicate that 2.4 water molecules are found within the first solvation shell when the well depth is ϵ_1, 7.4 when the well depth is $2\epsilon_1$, 13.2 when the well depth is $3\epsilon_1$, and 20.0 when the well depth is $4\epsilon_1$. These results are quite interesting because they suggest that the effective size of the surfactant heads (which is due to the association of water and/or counterions to the surfactant heads) determines the morphology of the surfactant aggregate at solid−liquid interfaces.

We finally quantified the average number of water molecules found in contact with the last five methyl groups in the surfactant

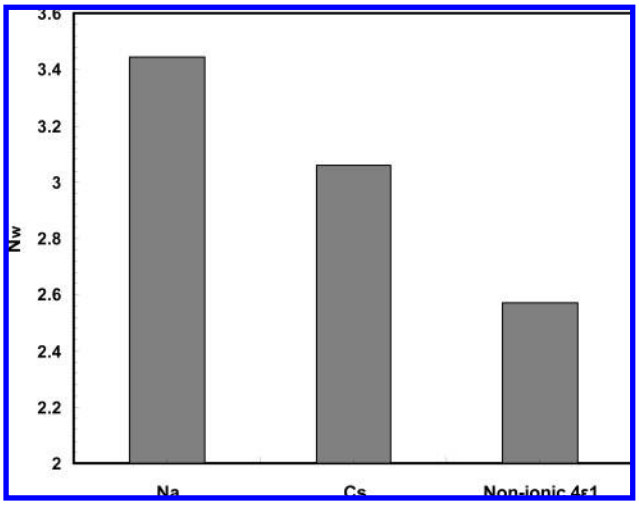

Figure 14. Average number of water molecules (N_w) within a radius of 0.5 nm from any of the five methyl groups farthest away from the surfactant heads. N_w for SDS surfactants in the presence of Na^+ and Cs^+ counterions is compared to that for nonionic SDS-like surfactants with strong head group−water interactions ($4\epsilon_1$).

tails in the various cases considered. The results are shown in Figure 14. The nonionic SDS-like surfactant with the strongest head group−water interaction is compared to the SDS surfactant when sodium or cesium ions act as counterions. As expected from the simulation snapshots shown above (compare Figure 5 to Figure 11 and to Figure 12), the average number of water molecules in contact with the hydrophobic surfactant tails decreases as the surface aggregates resemble more and more the perfect hemi-cylinders of Figure 8a.

Conclusions

We conducted a number of molecular dynamics simulations to study the self-assembly of SDS surfactants at the graphite−water interface. We reported a comprehensive set of results obtained for surfactants adsorbed on two opposed graphite surfaces as the distance between the surfaces varies from 14.0 to 4.05 nm. We employed distribution functions between sodium and sulfur and sulfur and sulfur as well as mean square displacement data and population distributions for the surfactant length to analyze the effect of the frontal confinement on the surface aggregates. Our results suggest the presence of surface aggregate−surface aggregate interactions when the distance between opposing graphite surfaces is less than 10.0 nm. At separations approaching twice the surface aggregate thickness we observe an effective attraction between head groups of surfactants adsorbed on the opposing surfaces. At separations above four times the surface aggregate thickness (>8 nm) the surface structures do not seem to depend on the presence of surfactant aggregates on the opposing surface.

Within the limitations of the state-of-the-art computational facilities, which allow us to conduct all-atom molecular dynamics simulations for up to 10−20 ns in systems as complicated as those considered here, the morphology of the surfactant aggregates was studied in great detail. Our results show that when aqueous SDS surfactants are considered, counterion condensation is responsible for the formation of dense patches composed by surfactant heads and counterions. Because these patches are very dense, some hydrophobic surfactant tails remain exposed to water. When the sodium counterions are substituted with the larger cesium counterions, most of the surfactant tails are shielded from the aqueous solution and the self-assembled aggregate resembles a perfect hemi-cylinder.

We conducted a parametric study on nonionic SDS-like surfactants to further unveil the role of counterion condensation on determining the morphology of the surfactant aggregates. We found a number of surface structures (layered structures, raising pancakes, and perfect hemi-cylinders) as the hydrophilicity of the surfactant head group was changed. The change of surface aggregate structure of SDS molecule from partial hemi-cylinder to perfect hemi-cylinder when sodium counterions are replaced by cesium counterions happened within ~2 ns in our simulations. The surface aggregate structure of nonionic model SDS surfactants with maximum hydrophilicity yields perfect hemi-cylinders. Even this phenomenon occurs in time scales accessible to all-atom molecular dynamics, in this case ~2 ns. This suggests that the change in equilibrium configuration resulting with the change in force field parameters is often accessible within 5−10 ns of all-atom MD simulations. To test whether the imperfect hemi-cylinders correspond to the equilibrium configuration for SDS surfactants at the graphite−water interface we assigned electric charges to the model nonionic surfactants. Following this inverse procedure we obtained surfactant aggregates with morphological features statistically identical to those observed originally for SDS aggregates within 2 ns, further corroborating the correctness of the procedure employed in our simulations. The results presented here provide significant insights into the importance of counterion condensation in determining the morphology of surface aggregates of amphiphilic molecules, a phenomenon that could be employed to control self-assembly processes toward the production of structures with practical interest. Further, the distribution functions provided can be used to develop coarse-grained models for studying surfactant self-assembly in larger systems.

Acknowledgment. Financial support was provided by the Oklahoma State Regents for Higher Education and the Vice President for Research at the University of Oklahoma, Norman, through a Junior Faculty Research Program award. Simulation calculations were performed at OSCER, Norman, OK, and at NERSC, Berkeley, CA. The authors wish to thank Dr. Brian Grady at the University of Oklahoma for frequent fruitful discussions.

References and Notes

(1) Beck, J. S.; Vartuli, J. C.; Roth, W. J.; Leonowicz, M. E.; Kresge, C. T.; Schmitt, K. D.; Chu, C. T. W.; Olson, D. H.; Sheppard, E. W.; McCullen, S. B.; Higgins, J. B.; Schlenker, J. L. *J. Am. Chem. Soc.* **1992**, *114*, 10834−10843.

(2) Marquez, M.; Patel, K.; Carswell, A.; Schmidtke, D. W.; Grady, B. P. *Langmuir* **2006**, *22*, 8010−8016.

(3) Marquez, M.; Grady, B. P. *Langmuir* **2004**, *20*, 10998−11004.

(4) Somasundaran, P.; Fuerstenau, D. W.; Healy, T. W. *J. Phys. Chem.* **1964**, *68*, 3562−3565.

(5) Somasundaran, P.; Fuerstenau, D. W. *J. Phys. Chem.* **1966**, *70*, 90−94.

(6) Wakamats, T.; Fuerstenau, D. W. *Adv. Chem. Ser.* **1968**, *79*, 161−176.

(7) Dick, S. G.; Fuerstenau, D. W.; Healy, T. W. *J. Colloid Interface Sci.* **1971**, *37*, 595−600.

(8) Ball, B.; Fuerstenau, D. W. *Discuss. Faraday Soc.* **1971**, *52*, 361−366.

(9) Trogus, F. J.; Schechter, R. S.; Pope, G. A.; Wade, W. H. *J. Petrol. Technol.* **1979**, *31*, 769−778.

(10) Nunn, C.; Schechter, R. S.; Wade, W. H. *J. Colloid Interface Sci.* **1981**, *80*, 598−605.

(11) Scamehorn, J. F.; Schechter, R. S.; Wade, W. H. *J. Am. Oil Chem. Soc.* **1983**, *60*, 1345−1349.

(12) Scamehorn, J. F.; Schechter, R. S.; Wade, W. H. *J. Colloid Interface Sci.* **1982**, *85*, 463−478.

(13) Somasundaran, P.; Middleton, R.; Viswanathan, K. V. *ACS Symp. Ser.* **1984**, *253*, 269−290.

(14) Viswanathan, K. V.; Somasundaran, P. *Colloid Surf.* **1987**, *26*, 19−41.

(15) Somasundaran, P.; Celik, M.; Goya, A.; Manev, E. *Soc. Petrol. Eng. J.* **1984**, *24*, 233−239.

(16) Levitz, P.; Vandamme, H. *J. Phys. Chem.* **1984**, *88*, 2228−2235.

(17) Levitz, P.; Vandamme, H. *J. Phys. Chem.* **1986**, *90*, 1302−1310.

(18) Levitz, P. *Langmuir* **1991**, *7*, 1595−1608.

(19) Manne, S.; Cleveland, J. P.; Gaub, H. E.; Stucky, G. D.; Hansma, P. K. *Langmuir* **1994**, *10*, 4409−4413.

(20) Warr, G. G. *Curr. Opin. Colloid Interface Sci.* **2000**, *5*, 88−94.

(21) Tiberg, F.; Brinck, J.; Grant, L. *Curr. Opin. Colloid Interface Sci.* **1999**, *4*, 411−419.

(22) Wanless, E. J.; Ducker, W. A. *J. Phys. Chem.* **1996**, *100*, 3207−3214.

(23) Isrealachvili, J. *Intermolecular and Surface Forces*, 2nd ed.; Academic Press: London, 1992.

(24) Shelley, J. C.; Shelley, M. Y. *Curr. Opin. Colloid Interface Sci.* **2000**, *5*, 101−110.

(25) Rajagopalan, R. *Curr. Opin. Colloid Interface Sci.* **2001**, *6*, 357−365.

(26) Lokar, W. J.; Koopal, L. K.; Leermakers, F. A. M.; Ducker, W. A. *J. Phys. Chem. B* **2004**, *108*, 15033−15042.

(27) Koopal, L. K.; Leermakers, F. A. M.; Lokar, W. J.; Ducker, W. A. *Langmuir* **2005**, *21*, 10089−10095.

(28) Leermakers, F. A. M.; Koopal, L. K.; Lokar, W. J.; Ducker, W. A. *Langmuir* **2005**, *21*, 11534−11545.

(29) Leermakers, F. A. M.; Koopal, L. K.; Goloub, T. P.; Vermeer, A. W. P.; Kijlstra, J. *J. Phys. Chem. B* **2006**, *110*, 8756−8763.

(30) Behjatmanesh-Ardakani, R. *J. Chem. Phys.* **2005**, *122*, 204903.

(31) Wijmans, C. M.; Linse, P. *J. Phys. Chem.* **1996**, *100*, 12583.

(32) Zhan, Y.; Mattice, W. L.; Napper, D. H. *J. Chem. Phys.* **1993**, *98*, 7502−7507.

(33) Zhan, Y.; Mattice, W. L.; Napper, D. H. *J. Chem. Phys.* **1993**, *98*, 7508−7514.

(34) Reimer, U.; Wahab, M.; Schiller, P.; Mogel, H.-J. *Langmuir* **2005**, *21*, 1640.

(35) Semler, J. J.; Genzer, J. *Macromol. Theory Simul.* **2004**, *13*, 219.

(36) Golumbfskie, A. J.; Pande, V. S.; Chakraborty, A. K. *Proc. Natl. Acad. Sci. U.S.A.* **1999**, *96*, 11707.

(37) Bratko, D.; Chakraborty, A. K.; Shakhnovich, E. I. *J. Chem. Phys.* **1997**, *106*, 1264.

(38) Seok, C.; Freed, K. F.; Szleifer, I. *J. Chem. Phys.* **2000**, *112*, 6443.

(39) Fleer, C. J.; Scheutjens, J. *Colloid Surf.* **1990**, *51*, 281.

(40) Semler, J. J.; Genzer, J. *J. Chem. Phys.* **2003**, *119*, 5274.

(41) Larson, R. G. *J. Chem. Phys.* **1989**, *91*, 2479.

(42) Larson, R. G. *J. Chem. Phys.* **1992**, *96*, 7904.

(43) Larson, R. G. *Chem. Eng. Sci.* **1994**, *49*, 2833.

(44) Care, C. M. *J. Chem. Soc., Faraday Trans.* **1987**, *83*, 2905.

(45) Brindle, D.; Care, C. M. *J. Chem. Soc., Faraday Trans.* **1992**, *88*, 2163.

(46) Desplat, J.-C.; Care, C. M. *Mol. Phys.* **1996**, *87*, 441.

(47) Rodrigues, K.; Mattice, W. L. *J. Chem. Phys.* **1991**, *95*, 5341.

(48) Wijmans, C. M.; Linse, P. *Langmuir* **1995**, *11*, 3748.

(49) Fodi, B.; Hentschke, R. *Langmuir* **2000**, *16*, 1626.

(50) Reimer, U.; Wahab, M.; Schiller, P.; Mogel, H.-J. *Langmuir* **2001**, *17*, 8444.

(51) Cabral, V. F.; Abreu, C. R. A.; Castier, M.; Tavares, F. W. *Langmuir* **2003**, *19*, 1429.

(52) Zhan, Y.; Mattice, W. L. *Macromolecules* **1994**, *27*, 683.

(53) Wijmans, C. M.; Linse, P. *J. Chem. Phys.* **1997**, *106*, 328.

(54) Bocker, J.; Schlenkrich, M.; Bopp, P.; Brickmann, J. *J. Phys. Chem.* **1992**, *96*, 9915.

(55) Shelley, J. C.; Patey, G. N. *Mol. Phys.* **1996**, *88*, 385.

(56) Schweighofer, K. J.; Essmann, U.; Berkowitz, M. *J. Phys. Chem. B* **1997**, *101*, 3793−3799.

(57) Dominguez, H.; Berkowitz, M. L. *J. Phys. Chem. B* **2000**, *104*, 5302−5308.

(58) Ibrahim, T. H.; Neuman, R. D. *Langmuir* **2004**, *20*, 3114−3122.

(59) Cooper, T. G.; de Leeuw, N. H. *Langmuir* **2004**, *20*, 3984.

(60) Salaniwal, S.; Cui, S. T.; Cummings, P. T.; Cochran, H. D. *Langmuir* **1999**, *15*, 5188.

(61) Salaniwal, S.; Cui, S. T.; Cochran, H. D.; Cummings, P. T. *Ind. Eng. Chem. Res.* **2000**, *39*, 4543.

(62) Salaniwal, S.; Cui, S. T.; Cochran, H. D.; Cummings, P. T. *Langmuir* **2001**, *17*, 1773.

(63) Shah, K.; Chiu, P.; Jain, M.; Fortes, J.; Moudgil, B.; Sinnott, S. *Langmuir* **2005**, *21*, 5337.

(64) Bandyopadhyay, S.; Shelley, J. C.; Tarek, M.; Moore, P. B.; Klein, M. L. *J. Phys. Chem. B* **1998**, *102*, 6318.

(65) Dominguez, H. *J. Phys. Chem. B* **2007**, *111*, 4054−4059.

(66) Bruce, C. D.; Berkowitz, M. L.; Perera, L.; Forbes, M. D. E. *J. Phys. Chem. B* **2002**, *106*, 3788−3793.

(67) Greenwood, F. G.; Parfitt, G. D.; Picton, N. H.; Wharton, D. G. In *Adsorption from Aqueous Solution*; Weber, W. J., Matijevic, E., Eds.; American Chemical Society: Washington, DC, 1968; pp 135−144.

(68) Berendsen, H. J. C.; Grigera, J. R.; Straatsma, T. P. *J. Phys. Chem.* **1987**, *91*, 6269−6271.
(69) Chang, A.; Steele, W. A. *J. Chem. Phys*. **1990**, *92*, 3858−3866.
(70) Ryckeart, J. P.; Bellemans, A. *Chem. Phys. Lett*. **1975**, *123*, 30.
(71) Předota, M.; Bandura, A. V.; Cummings, P. T.; Kubicki, J. D.; Wesolowski, D. J.; Chialvo, A. A.; Machesky, M. L. *J. Phys. Chem. B* **2004**, *108*, 12061−12072.
(72) Smith, E. D.; Dang, L. X. *J. Chem. Phys*. **1994**, *101*, 7873−7881.
(73) Gao, J.; Ge, W.; Hu, G.; Li, J. *Langmuir* **2005**, *21*, 5223−5229.
(74) Lu, J. R.; Marrocco, A.; Su, T. J.; Thomas, R. K.; Penfold, J. *J. Colloid Interface Sci*. **1993**, *158*, 303−316.
(75) Plimpton, S. J. *J. Comput. Phys.* **1995**, *117*, 1−19, http://lammps.sandia.gov.
(76) Allen, M. P. Tildesley, D. J. *Computer Simulation of liquids*; Oxford University Press: Oxford, 1987.
(77) Bitting, D.; Harwell, J. H. *Langmuir* **1987**, *3*, 500−511.